ACCSCIENCE PUBLISHING

International Journal of Bioprinting

RESEARCH ARTICLE

Self-healing silk fibroin–gelatin–based 3D-printed bilayer scaffolds with stable interface and bidirectional lineage control for osteochondral regeneration

Hong Liu[1], Danyu Yao[1,2*], Ling Wang[1,2*], and Mingen Xu[1,2*]

[1]School of Automation, Hangzhou Dianzi University, Hangzhou, Zhejiang, China

[2]Zhejiang Key Laboratory of Medical Additive Manufacturing and Information Fusion, Hangzhou, Zhejiang, China

Abstract

The osteochondral interface—characterized by a steep gradient in both composition and mechanical properties—remains one of the most challenging anatomical sites to regenerate. Reconstructing this spatially complex heterogeneity continues to confound conventional osteochondral grafts. Although multilayer scaffolds are widely adopted, interfacial delamination frequently compromises repair outcomes. Here, we report a self-healing, physically crosslinked silk fibroin–based 3D-printing ink that incorporates gelatin and nano-hydroxyapatite for the fabrication of bilayer scaffolds with robust interfacial bonding. By tuning ultrasonication time of silk fibroin and gelatin content, the ink exhibits exceptional printability and cytocompatibility, enabling >90% post-printing cell viability. Leveraging a dual-nozzle alternating-print strategy, we generated bilayer constructs that display a stable interface and layer-specific mechanical heterogeneity. Both upper- and lower-layer inks possess good self-healing capacity, eliminating delamination and yielding a monolithic scaffold. Functional analyses revealed significant upregulation of the chondrogenic marker type II collagen in the upper layer and the osteogenic marker RUNX2 in the lower layer, achieving bidirectional lineage instruction required for osteochondral regeneration. This silk/gelatin-based, physically crosslinked, integrative bilayer scaffold offers a promising therapeutic platform for osteochondral defect repair.

Keywords: Silk fibroin; Cell-laden 3D printing; Self-healing Bioink; Bilayer scaffold; Osteochondral repair

***Corresponding authors:**
Danyu Yao
(yaodanyu@hdu.edu.cn)
Ling Wang
(lingw@hdu.edu.cn)
Mingen Xu
(xumingen@hdu.edu.cn)

Citation: Liu H, Yao D, Wang L, Xu M. Self-healing silk fibroin–gelatin–based 3D-printed bilayer scaffolds with stable interface and bidirectional lineage control for osteochondral regeneration. *Int J Bioprint.* 2026:12(2):026050034. doi: 10.36922/IJB026050034

Received: January 27, 2026

Revised: March 8, 2026

Accepted: March 10, 2026

Published online: April 3, 2026

1. Introduction

Osteochondral tissue serves as the core functional unit of the joint system, with its unique gradient heterogeneous structure endowing the joint with exceptional compressive resistance, shock-absorbing capacity, and movement coordination.[1,2] However, Osteochondral interface often suffers from defects due to trauma (*e.g.*, sports injuries, traffic accidents), degenerative diseases (*e.g.*, osteoarthritis), or physiological aging. These defects lead to the degradation of hyaline cartilage matrix or the destruction of

subchondral bone microstructure, ultimately manifesting as joint pain, limited mobility, and even loss of motor function in severe cases.[3] Hyaline cartilage has extremely weak self-repair ability after injury due to the lack of vascular, neural and lymphatic supply. Once a defect occurs, without timely intervention, it is prone to gradual progression to irreversible joint dysfunction, imposing a heavy burden on patients' quality of life and the social medical system.[4,5]

Traditional therapeutic approaches, such as microfracture and autologous cartilage transplantation, struggle to meet the clinical demand for long-term effective repair—either because the regenerated tissue is mostly fibrocartilage (characterized by poor mechanical properties and high susceptibility to degradation) or due to limited donor sources and the risk of donor site morbidity. Tissue engineering technology, relying on the synergistic strategy of "scaffold-cell-bioactive factor," has emerged as a core research direction to break through the bottlenecks of traditional treatments.[6,7] Nevertheless, the gradient heterogeneity and interfacial continuity of osteochondral tissue pose rigorous challenges to scaffold design: the cartilage layer requires a microenvironment with high hydrophilicity, and the ability to promote chondrocyte phenotype maintenance, while the subchondral bone layer needs to meet the requirements of high mechanical strength, osteoconductivity, and osteoblast differentiation-inducing capacity.[8,9] This has rendered biphasic scaffolds that mimic the hierarchical structure of natural osteochondral tissue a research focus. However, traditional bilayer scaffolds are mostly fabricated via layer-by-layer casting or physical stacking.[10,11] Differences in swelling ratio and degradation rate between interlayer materials often result in weak interface bonding, ultimately leading to tissue separation between regenerated cartilage and subchondral bone, which severely restricts the repair efficacy.[12,13]

The emergence of 3D printing technology has provided a new approach to addressing this challenge.[14] Compared with traditional fabrication methods, 3D printing can achieve digital customization of scaffold structures and precise construction of functional gradients by accurately regulating printing paths, ink compositions, and crosslinking methods. However, the performance of bioinks remains the core factor determining the quality of 3D-printed scaffolds, and the performance discrepancies and interface integration between heterogeneous materials are still the major bottlenecks limiting their clinical application.[15,16] Notably, constructing a bilayer scaffold utilizing the same base material system not only ensures the biocompatibility and mechanical tunability of the material but also achieves seamless interlayer connection through material continuity, self-healing, *etc.*, effectively avoiding interface separation and holding great promise for enhancing repair outcomes.[17,18]

Among various bioink materials, the composite of silk fibroin (SF) and gelatin has attracted considerable attention due to its inherent advantages. Silk fibroin exhibits remarkable bioactivity and tunable mechanical properties. By regulating its secondary structure (*e.g.*, β-sheet content), the elastic modulus and degradation rate of scaffolds can be optimized to meet the requirements of both cartilage and bone tissues.[19,20] However, 3D printing using SF alone faces significant challenges: untreated SF solutions have low viscosity, failing to meet the rheological requirements for extrusion printing, while inducing β-sheet crystallization often leads to nozzle clogging due to localized gel aggregation and increased brittleness, thereby compromising printing continuity.[21-23] As a partial hydrolysis product of collagen, gelatin not only inherits the cell compatibility of collagen but also can improve the rheological behavior of the bioink by adjusting temperature and concentration, thereby enhancing printability and shape fidelity.[24,25] The composite of SF and gelatin enables the synergistic optimization of "printing performance-bioactivity" and is often used to construct cartilage scaffolds.[26] The active groups such as amino and hydroxyl groups on the SF molecular chains can form multiple intermolecular forces (hydrogen bonds, hydrophobic interactions, *etc.*) with the peptide bonds in gelatin molecules, which provides a natural molecular basis for the realization of self-healing performance of composite inks—when micro-damages occur in the ink due to extrusion shear, interfacial contact and other factors, these intermolecular forces can drive the recombination of molecular chains at the damaged sites to complete the autonomous structural repair. This allows the ink to not only meet the extrusion fluidity requirements for 3D printing but also strengthen the interlayer bonding through the self-healing effect. Photosensitive modified SF-gelatin mixtures for 3D-printed scaffold construction have been reported.[27,28] Notably, most conventional scaffolds tend to induce cellular spreading, which in turn stimulates the excessive deposition of fibrous matrix—an outcome that is incompatible with the cellular microenvironment required for cartilage repair. Cell-encapsulated scaffolds are favorable for maintaining the spherical morphology and functional phenotype of chondrocytes, making them an ideal choice for cartilage tissue engineering.[29,30] However, in the specific application scenario of cell-laden bioprinting, existing solidification strategies still have critical bottlenecks that urgently need to be addressed: chemical crosslinkers may exert cytotoxic effects, while

photoinitiators combined with ultraviolet (UV) irradiation are prone to impairing cell viability, making it difficult to meet the core requirement of "instant print-and-culture." Therefore, there is currently a lack of a mild solidification strategy that possesses excellent biocompatibility, supports cell survival and phenotype maintenance, and is suitable for the SF/gelatin system. It is imperative to improve the preparation technology of SF/gelatin composite inks and develop a cell-laden bioink with good biocompatibility that does not require UV irradiation or toxic crosslinkers, thereby promoting its direct application in 3D bioprinting for cartilage repair.

In our previous studies, we found that crystalline SF can induce the self-assembly of untreated SF. This self-assembly process is synergistically driven by intermolecular hydrogen bonding and hydrophobic interactions, enabling the rapid formation of physically crosslinked hydrogels with stable structures.[31] Notably, the gelation time can be regulated by adjusting the proportion of crystalline SF. Meanwhile, ultrasonic treatment is a green and non-toxic physical method for inducing the formation of crystalline SF. The combination of ultrasonic treatment and SF self-assembly can accelerate the gelation process of SF, offering potential for constructing cell-friendly scaffolds. Furthermore, hydroxyapatite (HAP) is the main inorganic component of bone, possesses excellent osteoconductivity and osteoinductivity, and is often used to enhance the osteogenic activity of scaffolds.[32,33] Based on this, this work proposes an improved physical crosslinking strategy: using SF–gelatin as the matrix, the gelation and solidification process of the bioink is regulated by adjusting the ink composition and ultrasonic treatment conditions to prepare the cartilage layer bioink that can directly load cells; HAP particles are uniformly dispersed in the SF–gelatin system to construct a bone layer bioink with osteogenic activity.

In this study, a physically crosslinked protein-based bioink with self-healing properties was developed to construct bilayer scaffolds with strong interfacial adhesion. A non-toxic and controllable physically crosslinked bioink was fabricated based on ultrasound induction. The composition and preparation process of the SF–gelatin–based ink were systematically regulated, and its rheological properties and printability were optimized to determine the optimal formulations for the chondral layer and osseous layer inks. A dual-nozzle 3D printing technique was employed to construct osteochondral integrated bilayer scaffolds with both self-healing characteristics and stable interfaces. The swelling stability, mechanical heterogeneity, and interlayer structural continuity of the scaffolds were systematically characterized. *In vitro* cellular experiments using separate seeding of ATDC5 cells and bone marrow-derived mesenchymal stem/stromal cells (BMSCs) verified the excellent biocompatibility and bidirectional osteochondral lineage regulation ability of the scaffolds (Figure 1). Ultimately, this work provides a novel tissue engineering strategy for the functional repair of osteochondral interface defects, featuring non-toxic crosslinking, high interfacial integration, and precise functional differentiation.

2. Materials and methods

2.1. Preparation of silk fibroin solution

Anhydrous sodium carbonate weighing 4.24 g was added to boiled deionized water. Then, 10 g of silk fiber (Jiaxin, China) was weighed and immersed in the solution, followed by boiling for 30 min. The treated silk was rinsed with deionized water 5–6 times and then placed in an oven at 60 °C for overnight drying. The dried silk fiber was immersed in a 9.3 M lithium bromide solution and incubated in an oven at 60 °C for 4–6 h until complete dissolution was achieved. The resulting solution was transferred into a dialysis bag (3500 kDa) and dialyzed for 3 days. After dialysis, the solution was centrifuged to remove insoluble components, and the silk fibroin solution (SF) was finally obtained.

2.2. Sonication treatment

Six milliliters of silk fibroin/gelatin-based aqueous solution were placed into a 10 mL test tube, which was then transferred to a constant-temperature water bath for preheating and temperature-controlled incubation at 37 °C for 30 min. Subsequent to preheating, a probe-type (conical) ultrasonic cell disruptor was employed to subject the solution to ultrasonic treatment, with the instrument operating at a full power of 650 W and an output power of 10%. The ultrasonic mode was set to a cyclic pattern of 2 s on and 2 s off, and the total duration of ultrasonic treatment was controlled within the range of 20–150 s. Upon completion of ultrasonic treatment, the resulting solution was moved to a high-pressure sterilization device and sterilized at 120 °C and 0.1 MPa for 15 min. After the solution was cooled to room temperature, it was stored in a 4 °C refrigerator for subsequent use.

2.3. Preparation of bioinks

2.3.1. Preparation of the upper-layer inks (SSF/GEL)

Gelatin (GEL) particles (Aladdin, China) were weighed and dissolved in deionized water to prepare gelatin solutions. Specifically, 3% w/v gelatin solution was mixed with 4% w/v, 5% w/v, and 6% w/v SF solutions at a volume

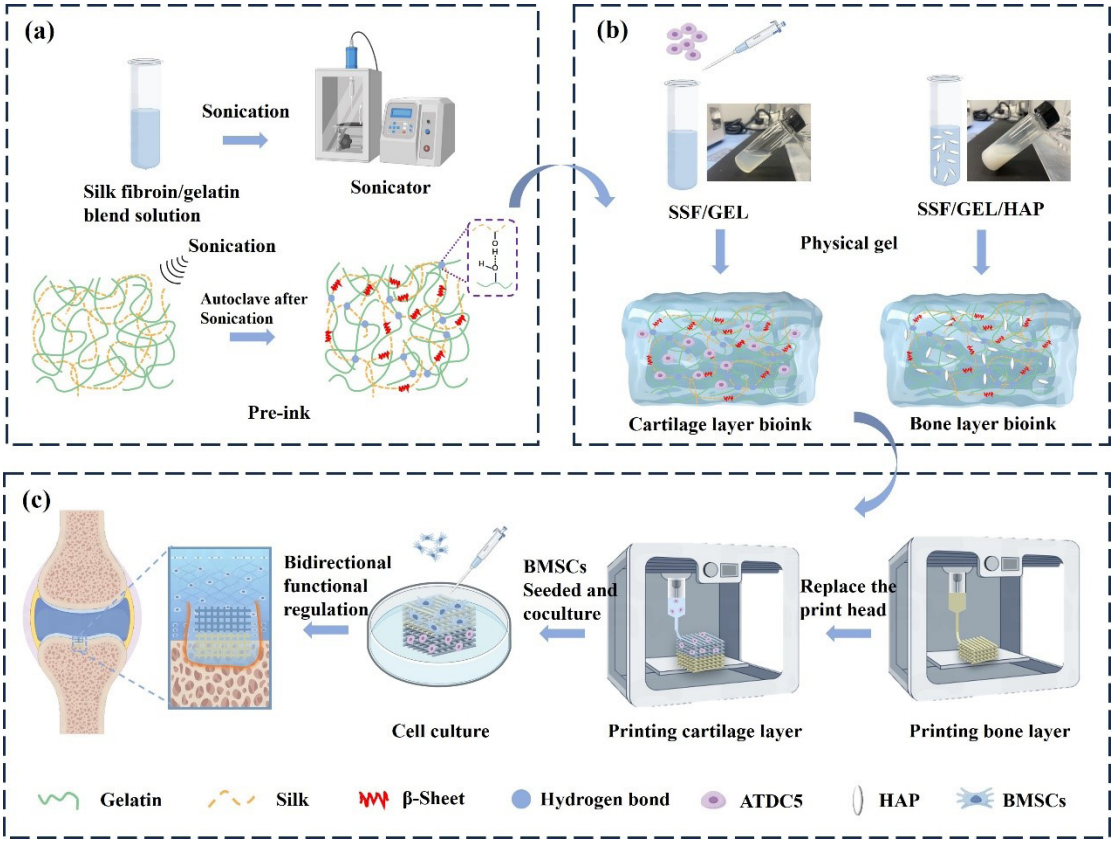

Figure 1. Schematic diagram of the construction of the physically crosslinked silk fibroin–gelatin bilayer scaffold for osteochondral repair. (a) Silk fibroin and gelatin solutions were mixed and treated with ultrasound, by which silk fibroin was induced to form a β-sheet structure; meanwhile, some hydrogen bonds were formed between hydrophilic groups. (b) Before the silk fibroin–gelatin solution was gelled, ATDC5 cells suspension was added into it and mixed uniformly, by which cartilage ink was constructed; HAP was incorporated into the silk fibroin-gelatin solution, and thus bone layer ink was formed. (c) A dual-nozzle 3D printing technique was adopted for the fabrication of the bilayer scaffold: the bone layer scaffold was printed first, followed by the direct printing of the cartilage layer scaffold on it; finally, BMSCs were seeded onto the upper surface of the bone layer scaffold, and subsequent culture was performed for biological detection.
Abbreviations: BMSCs: Bone marrow-derived mesenchymal stem cells; GEL: Gelatin; HAP: Hydroxyapatite; SSF: Sonicated silk fibroin.

ratio of 1:1, respectively. Additionally, 6% w/v SF solution was mixed with 2% w/v, 3% w/v, 5% w/v, 8% w/v, and 10% w/v gelatin solutions at a volume ratio of 1:1, respectively. The above mixture was subjected to ultrasonic treatment (10% power) using a cell disruptor (Shunliu Instrument Company, China), after sterilization, the cartilage layer bioinks labeled as 2SSF/1.5GEL, 2.5SSF/1.5GEL, 3SSF/1GEL, 3SSF/1.5GEL, 3SSF/2.5GEL, 3SSF/4GEL, and 3SSF/5GEL were obtained (Table 1).

2.3.2. Preparation of lower-layer inks (SSF/GEL/HAP)

HAP nanoparticles (Aladdin, China) were doped into the 3% w/v gelatin solution at mass ratios of 5 wt%, 10 wt%, and 20 wt%. Each mixture was subjected to ultrasonic treatment at 10% power using an ultrasonic cell disruptor to homogenize the HAP nanoparticles. Subsequently, the HAP-gelatin composite solution was mixed with 6% w/v SF solution at a volume ratio of 1:1, subjected to ultrasonic treatment again. Finally, the resulting solution was autoclaved, yielding the bone layer bioinks labeled as 3SSF/1.5GEL/5HAP, 3SSF/1.5GEL/10HAP, and 3SSF/1.5GEL/20HAP (Table 1).

2.4. X-ray diffraction

After freeze-drying, the samples were sectioned and placed on glass slides. The crystal structure of the sample was determined using an X-ray diffractometer (XRD, Rigaku Ultima IV, Rigaku, Japan) at a tube voltage of 40 kV and a tube current of 30 mA, with a diffraction angle (2θ) range of 10°–40° and a scanning speed of 20°/min.

Table 1. Formulation and composition of the bioink

Bioink	SSF (% w/v)	GEL (% w/v)	HAP (wt%)	Sonication time (s)
2SSF/1.5GEL	2.0	1.5	0	80
2.5SSF/1.5GEL	2.5	1.5	0	60
3SSF/1GEL	3.0	1.0	0	40
3SSF/1.5GEL	3.0	1.5	0	50
3SSF/2.5GEL	3.0	2.5	0	70
3SSF/4GEL	3.0	4.0	0	120
3SSF/5GEL	3.0	5.0	0	150
3SSF/1.5GEL/5HAP	3.0	1.5	5	120
3SSF/1.5GEL/10HAP	3.0	1.5	10	120
3SSF/1.5GEL/20HAP	3.0	1.5	20	120

Abbreviations: GEL: Gelatin; HAP: Hydroxyapatite; SSF: Sonicated silk fibroin.

2.5. Rheological analysis

After ultrasonic treatment (3–5 h, after bioink gelation), a rheometer (MARS40; HAAKE, Germany) was used to conduct the following experiments. The gap between the rotor and the bottom plate was maintained at 1 mm, the operating temperature was set according to Table 2, and the relevant tests were initiated after 5 min of temperature equilibration: (i) Rotational shear rate sweep tests were conducted to evaluate viscosity and shear-thinning behavior (shear rate range: 0.1–100 s^{-1}). (ii) Oscillatory amplitude sweep tests were performed to assess the solid-like behavior and linear viscoelastic region of the inks through storage modulus (G') and loss modulus (G") measurements (strain range: 1–100%, frequency: 1 Hz). (iii) Cyclic strain amplitude sweep test for evaluating the self-healing ability of the bioink (the strain was alternately switched from a large strain [100%] to a small strain [10%] at an interval of 100 s for 3 cycles). (iv) Oscillatory temperature sweep tests were performed to assess the storage modulus (G') and loss modulus (G") under varying temperatures (temperature range: 0–40 °C, cooling rate: 2 °C/min, frequency: 1 Hz).

2.6. Preparation of 3D-printed scaffolds

3D-printed scaffolds were fabricated using a bioprinting platform (Regenovo, China). Cubic porous scaffolds (dimensions: 10 × 10 × 2 mm^3, 4 layers) were printed with SSF/GEL/HAP bioink and SSF/GEL bioink, respectively. A 90° cross-network structure was adopted for printing, with a printing speed of 15 mm/s, a printing spacing of 1.25 mm and a layer height of 0.25 mm. The fabrication process of the bilayer scaffold was as follows: First, the printing cartridges loaded with SSF/GEL/HAP bioink and SSF/GEL bioink were mounted on the 3D bioprinter. Based on the thermosensitive property of gelatin, an appropriate printing temperature was selected to ensure the high-fidelity printed structure of the scaffolds. The printing parameters were set according to Table 2, and the printing nozzles were calibrated prior to printing. The SSF/GEL/HAP layer scaffold (dimensions: 10 × 10 × 1 mm^3, 4 layers) was printed layer by layer. Subsequently, the printer head was switched to the one loaded with SSF/GEL bioink, and the SSF/GEL scaffold (dimensions: 10 × 10 × 1 mm^3, 4 layers) was printed layer by layer on the surface of the pre-printed SSF/GEL/HAP layer scaffold.

2.7. Mechanical properties of printed scaffolds

The printed samples were immersed in phosphate-buffered saline (PBS) solution at 37 °C. The compressive modulus of the scaffolds was measured using a universal testing machine (Dongri Instruments, China) equipped with a 100 N force sensor at room temperature. The thickness and basal area of each sample (dimensions: 10 × 10 × 2 mm^3) were measured prior to the test, and the samples were compressed at a strain rate of 2 mm/min at room temperature with the compressive strain range set to 0–50%. The compressive modulus of the samples was calculated based on the stress-strain curves within the 10% strain range.

2.8 Compression resilience tests

Cyclic loading unloading tests were conducted on the printed scaffolds using a mechanical tester (Dongri Instruments, China) to investigate their resilience. The thickness and bottom area of each sample (with dimensions of 10 × 10 × 2 mm^3) were measured. Compression

Table 2. Printing parameters of bioink

Bioink	Printing temperature (°C)	Printing pressure (MPa)	Needle diameter (mm)
2SSF/1.5GEL	12	0.12 ± 0.03	0.34
2.5SSF/1.5GEL	12	0.12 ± 0.02	0.34
3SSF/1GEL	10	0.1 ± 0.04	0.34
3SSF/1.5GEL	12	0.12 ± 0.02	0.34
3SSF/2.5GEL	15	0.22 ± 0.02	0.34
3SSF/4GEL	20	0.22 ± 0.03	0.34
3SSF/5GEL	25	0.22 ± 0.02	0.34
3SSF/1.5GEL/5HAP	12	0.1 ± 0.04	0.41
3SSF/1.5GEL/10HAP	12	0.1 ± 0.04	0.41
3SSF/1.5GEL/20HAP	12	0.1 ± 0.05	0.41

Abbreviations: GEL: Gelatin; HAP: Hydroxyapatite; SSF: Sonicated silk fibroin.

was applied at a constant rate of 2 mm/min at room temperature. After reaching a compressive strain of 25%, the samples were unloaded until a small load of 0.1 N was achieved. Each subsequent cycle commenced immediately after the previous one, and five loading unloading cycles were performed for each specimen.

2.9. Scanning electron microscopy

To observe the interfacial bonding of the bilayer scaffold, the samples were first rapidly frozen in liquid nitrogen followed by freeze-drying. Subsequently, the freeze-dried samples were sectioned with a surgical scalpel, and the sections were fixed on the SEM sample stage and uniformly sputter-coated with a layer of gold. Finally, the microstructure of samples (with a focus on the interfacial bonding region) was observed using a scanning electron microscope (SEM; JSM-7800F, JEOL, Japan) at an accelerating voltage of 5 kV.

2.10. Self-healing performance evaluation

2.10.1. Macroscopic morphology observation

To investigate the self-healing properties of the hydrogels, the hydrogel blocks of the cartilage layer and the bone layer were each cut into two pieces and placed back together, respectively. Meanwhile, one piece from each type of hydrogel block was spliced together, and self-healing was achieved without any external intervention.

2.10.2. Rheological recovery test

The hydrogels were placed on the parallel plate of a rheometer, and a strain amplitude sweep test was conducted on the osteochondral bioink at room temperature. The oscillatory strain amplitude was switched from a small strain of γ = 1.0% to a large strain of γ = 100%, with an interval of 100 s between each strain for a total of three cycles, so as to evaluate the self-healing performance of the osteochondral bioink.

2.11. Cell culture

Mouse chondrogenic cells (ATDC5; FH0378, FUHENG BIOLOGY, China) were cultured in DMEM/F12 medium, which was supplemented with 10% fetal bovine serum (FBS) (Sunview, China) and 1% penicillin-streptomycin mixture (TBD, USA). Rat (BMSCs were purchased from the Cell Bank of the Chinese Academy of Sciences (Shanghai, China, National Collection of Authenticated Cell Cultures) were cultured in α-MEM medium (Gibco, USA) supplemented with 10% FBS (Gibco, USA) and 1% penicillin-streptomycin mixture (TBD, USA). For the co-culture of ATDC5 cells and BMSCs, a mixed medium composed of α-MEM and DMEM/F12 at a volume ratio of 1:1 was used, with the addition of 10% FBS (Gibco, USA) and 1% penicillin-streptomycin mixture (TBD, USA). All cells were cultured in a constant-temperature incubator at 37 °C with 5% CO_2, and the culture medium was refreshed every two days.

2.12. Cell seeding

Different cell seeding strategies were adopted for the cartilage layer and bone layer scaffolds, respectively. For the cartilage layer, ATDC5 cells at a density of 1×10^6 cells/mL were pre-loaded into the printing bioink. The 3D-printed scaffolds (dimensions: $7 \times 7 \times 1$ mm^3) were directly placed into 24-well plates for culture. For the bone layer, BMSCs

were seeded onto the bone layer scaffolds (dimensions: 7 × 7 × 1 mm^3) at a density of 3×10^5 cells/mL. After 2 h of adhesion, the non-adherent cells were washed away, and the scaffolds were then transferred to new 24-well plates for subsequent culture.

2.13. CCK-8 assay

Cell proliferation was evaluated using a Cell Counting Kit-8 (CCK-8; Sunview, USA). The culture medium was refreshed every 2 days. After 1, 4, and 7 days of culture, the medium was removed. Subsequently, a working solution with a volume ratio of 10:1 (complete medium : CCK-8 reagent) was added to the 24-well plate. Each well received 300 μL of the working solution, and the plate was incubated in a 37 °C incubator for 2 h in the dark. Then, the reaction solution was transferred to a 96-well microplate, with 100 μL added to each well. Three blank control wells were set up for the assay. The optical density (OD) values were measured at a wavelength of 450 nm using a microplate reader (Varioskan ALF, Thermo Fisher Scientific, USA). The OD value was measured at a wavelength of 450 nm. The OD value of cells in the scaffold was obtained by calculating the difference in OD values between different samples and the control group, followed by averaging the results.

2.14. Live/Dead staining

Cell viability was assessed via the calcein-AM/PI double staining assay (K231206, KeyGEN, China). The staining solution was prepared by adding 1 μL of calcein-AM dye and 0.5 μL of propidium iodide (PI) dye to 1 mL of PBS. The culture medium was replaced every 2 days. After 1, 4 and 7 days of culture, 300 μL of the staining solution was added to each well, followed by incubation for 10 min at 37 °C in a cell incubator under light-protected conditions. After incubation, the working solution was aspirated, and the scaffolds were rinsed with PBS to remove residual working solution. Fluorescent images were then observed and captured using a confocal laser scanning microscope (A1RHD25, Nikon, Japan).

2.15. Immunofluorescence staining

After the samples were fixed with 4% paraformaldehyde (Beyotime, China) for 40 min, the cells were permeabilized with 0.5% Triton X-100 (OriLeaf, China) for 30 min, followed by three washes with PBS, 5 min each time. Blocking was performed with a blocking buffer consisting of 1% bovine serum albumin (BSA; Invitrogen, USA) and 0.5% Triton X-100 for 45 min. Subsequently, the samples were incubated overnight at 4 °C with primary antibodies, including mouse anti-RUNX2 and rabbit anti-collagen II (1:200; Boster, China). After washing with PBS, the samples were incubated for 2 h at 37 °C in the dark with a mixture of secondary antibodies: DyLight 488-conjugated goat anti-mouse and CY3-conjugated goat anti-rabbit (1:200; Boster, China). After washing with PBS, the cell nuclei were stained with DAPI nuclear staining solution (1:1000; Biosharp, USA) for 10 min. Finally, the samples were imaged using a confocal laser scanning microscope (Nikon, Japan).

2.16. Statistical analysis

All experimental data were tested in triplicate, and the results were expressed as the mean ± standard error of the mean (SEM). Statistical analyses were performed using Origin 2024 software (OriginLab Corporation, USA). One-way analysis of variance (ANOVA) was used to determine the significant differences between groups. Statistical significance was indicated as follows: $p < 0.05$, $p < 0.01$, and $p < 0.001$, where a value of $p < 0.05$ was considered statistically significant.

3. Results and discussion

3.1. Regulation of printing bioink

Mixing the cell suspension with a gel precursor solution to prepare cell-encapsulated pre-gel for 3D bioprinting is a widely adopted strategy in the field of bioprinting. A cell-compatible gelation induction method is an indispensable prerequisite for the realization of cell-laden bioprinting. Ultrasonic treatment is a well-established approach for the fabrication of SF hydrogels. Previous studies have demonstrated that incorporating cells into high-concentration SF solutions (>4% w/v) following ultrasonic treatment can effectively preserve cell viability,[34] which provides a feasible basis for the development of cell-laden SF-gelatin inks without the involvement of chemical crosslinkers.

Following ultrasonic treatment as described above, the SF-gelatin solution was immediately autoclaved to establish a sterile physically crosslinked system, which serves as a sterile cell carrier for subsequent cell experiments. Previous studies have demonstrated that high temperature promotes the conformational transition and self-assembly of SF molecular chains, thereby affecting the formation of β-sheets and the gelation rate. On this basis,[35,36] ultrasonic treatment can alter the hydrophobic hydration of SF via cavitation effects (local transient high temperature, high pressure, and high strain rate),[34] which modulate the hydrophobic hydration of SF molecules, accelerate the formation of β-sheet secondary structures,[31] and thereby facilitate the construction of physical crosslinking networks, ultimately achieving rapid sol-gel transition (Figure 2a).

As shown by the XRD results (Figure 2b), pure gelatin (GEL) and solution state SF exhibited broad diffuse peaks at 20.0° and 21.2°, respectively. These are typical characteristics of their amorphous random coil structure, with no obvious crystalline signals.[37] For the SF/gelatin blend (SF/GEL) before sonication, the main diffraction peak appeared at 20.6°, with a broadened shape and reduced intensity, indicating that SF existed mainly in a random coil conformation in the gelatin matrix and did not form a β-sheet structure. After sonication (SSF/GEL), the blend exhibited a diffraction peak at 20.9°, together with new shoulder peaks at 15.0° and 25.1°, suggesting the formation of β-sheet structures. Sonicated silk fibroin (SSF) showed distinct diffraction peaks at 16.2°, 20.5°, and 24.3°, which are characteristic signals of the β-sheet crystalline structure (silk II) of SF.[38] This confirmed that sonication successfully induced the conformational transition of silk fibroin from random coil to β-sheet. Compared with SSF, SSF/GEL exhibited broader and weaker peaks. This may be attributed to intermolecular forces such as hydrogen bonds formed between SF and gelatin, which disturbed the ordered arrangement of SF chains and resulted in decreased crystallinity of the β-sheet structure.[39]

We mainly investigated the effects of different SF/gelatin ratios, protein concentrations, and ultrasound treatment times on gel formation (Table 3). When the ultrasonic power was maintained constant (with an amplitude of 10%), the gelation time of SF-gelatin composites decreased with the increase in SF concentration (Figure 2c). This observation is consistent with previous findings, as the treatment of high-concentration solutions results in higher crosslinking density of SF, which favors hydrogel formation. In contrast, the gelation time was found to increase with the elevation of gelatin content (Figure 2d). Owing to the inability of low-concentration gelatin to form stable network structures at room temperature, the presence of gelatin in the mixed system hindered the gelation process. Among them, the 3SSF/5GEL group with the highest gelatin content remained in a liquid state

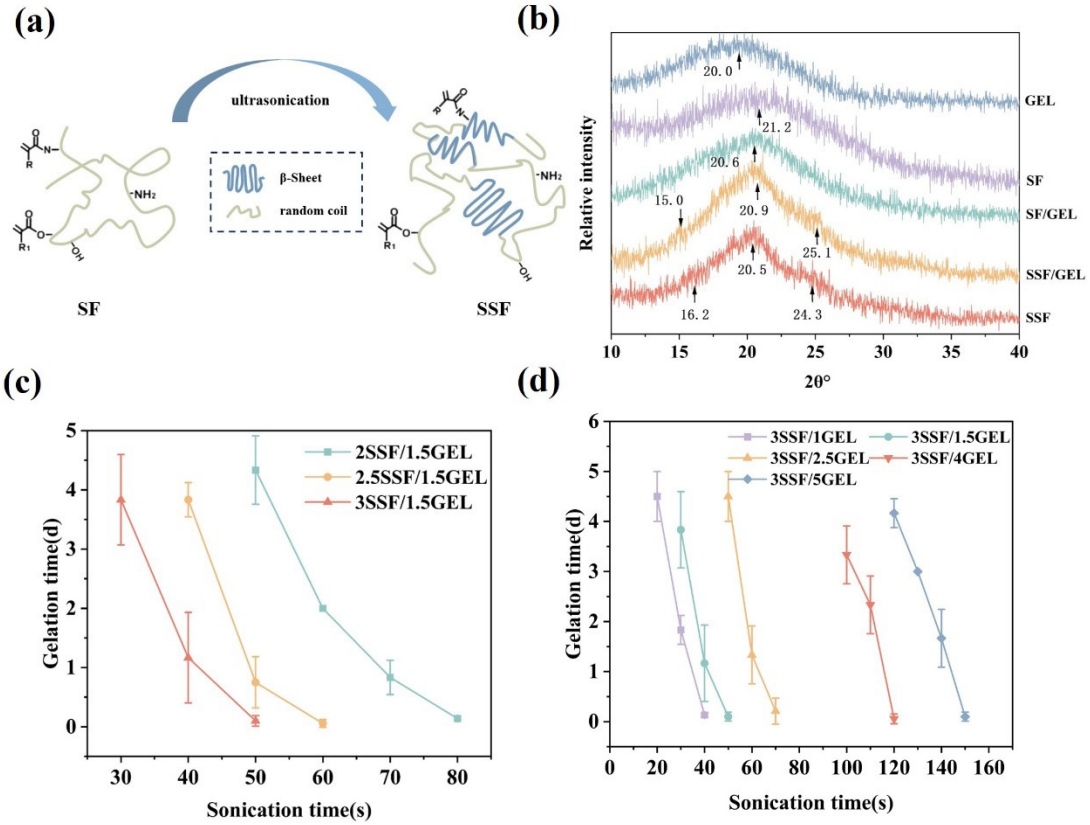

Figure 2. Effect of ultrasound treatment on ink structure and gelation time. (a) Schematic illustration of the mechanism by which ultrasound affects the structural changes of silk fibroin; (b) X-ray diffraction (XRD) characterization of the ink; (c) Gelation time of the ink under different silk fibroin concentrations and durations of ultrasound treatment; (d) Gelation time of the ink under different gelatin concentrations and durations of ultrasound treatment.

Abbreviations: GEL: Gelatin; SSF: Sonicated silk fibroin.

throughout the experiment, indicating that the SF content in this system was insufficient to support the formation of a stable three-dimensional network. Furthermore, the ultrasonic duration exerted a significant influence on the gelation time: when the ultrasonic duration was less than 40 seconds, all samples remained liquid; with the extension of ultrasonic duration, some samples were directly converted into solid gels after treatment.

Stable physical crosslinked gels could be obtained by incubating the ultrasonically treated solutions at room temperature for a certain period (Figure 3a). Temperature sweep test results showed that, before ultrasonic treatment, the modulus and viscosity of the ink decreased significantly with increasing temperature, exhibiting obvious thermosensitive characteristics. After ultrasonic treatment, the modulus and viscosity of the SSF/GEL ink remained essentially stable over the tested temperature range, and its storage modulus (G′), loss modulus (G″), and viscosity were significantly higher than those of the pristine ink (Figure 3b and 3c). These results indicate that the ultrasonically treated ink displayed attenuated temperature sensitivity. The enhanced modulus and viscosity of the ink are beneficial for improving the structural stability of printed constructs. By precisely regulating ultrasonic duration and SF-gelatin mass ratio, the gelation time of the ink can be tailored within the range of 3–5 h, which provides optimal conditions for subsequent 3D printing operations and *in vitro* cell culture.

In the osteochondral repair system, significant differences exist in the performance requirements between the lower-layer and upper-layer scaffolds. On one hand, the lower-layer scaffold must adapt to the mechanical microenvironment of bone tissue; on the other hand, it sustains the load of the upper layer, thereby imposing higher demands on mechanical strength. The incorporation of HAP into the bioink not only augments the mechanical robustness of the scaffold but also endows it with superior osteoinductive potential. In the present study, the SSF/GEL/HAP bone layer scaffolds were constructed via the introduction of HAP with varying mass fractions into the SSF/GEL bioink.

3.2. Printability analysis of bioink

SSF/GEL cartilage layer bioinks with gradient concentrations (gelatin: 1%–5% w/v; silk fibroin: 2%–3% w/v) and SSF/GEL/HAP bone layer bioinks

Table 3. The state and gelation time of the SSF/GEL ink under different ultrasonic durations

Ultrasound time (s)	Time (days) and physical state of the SSF/GEL ink gel after ultrasonic treatment						
	2SSF/1.5GEL	2.5SSF/1.5GEL	3SSF/1GEL	3SSF/1.5GEL	3SSF/2.5GEL	3SSF/4GEL	3SSF/5GEL
20	>7 (L)	>7 (L)	4.50 ± 0.50 (L)	>7 (L)	>7 (L)	>7 (L)	>7 (L)
30	>7 (L)	>7 (L)	1.83 ± 0.29 (L)	3.83 ± 0.76 (L)	>7 (L)	>7 (L)	>7 (L)
40	>7 (L)	3.83 ± 0.29 (L)	0.13 ± 0.04 (L)	1.17 ± 0.76 (L)	>7 (L)	>7 (L)	>7 (L)
50	4.33 ± 0.58 (L)	0.75 ± 0.43 (L)	0 (S)	0.17 ± 0.04 (L)	4.50 ± 0.50 (L)	>7 (L)	>7 (L)
60	1.83 ± 0.29 (L)	0.13 ± 0.08 (L)	0 (S)	0 (S)	1.33 ± 0.76 (L)	>7 (L)	>7 (L)
70	0.83 ± 0.29 (L)	0 (S)	0 (S)	0 (S)	0.17 ± 0.07 (L)	>7 (L)	>7 (L)
80	0.14 ± 0.02 (L)	0 (S)	0 (S)	0 (S)	0 (S)	>7 (L)	>7 (L)
90	0 (S)	0 (S)	0 (S)	0 (S)	0 (S)	>7 (L)	>7 (L)
100	0 (S)	0 (S)	0 (S)	0 (S)	0 (S)	2.83 ± 0.19 (L)	>7 (L)
110	0 (S)	0 (S)	0 (S)	0 (S)	0 (S)	2.33 ± 0.58 (L)	>7 (L)
120	0 (S)	0 (S)	0 (S)	0 (S)	0 (S)	0.18 ± 0.06 (L)	4.17 ± 0.29 (L)
130	0 (S)	0 (S)	0 (S)	0 (S)	0 (S)	0 (S)	2.83 ± 0.29 (L)
140	0 (S)	0 (S)	0 (S)	0 (S)	0 (S)	0 (S)	1.67 ± 0.58 (L)
150	0 (S)	0 (S)	0 (S)	0 (S)	0 (S)	0 (S)	0.14 ± 0.03 (L)

Notes: Physical state is denoted by either 'L' (solution state) or 'S' (gel state).
Abbreviations: GEL: Gelatin; SSF: Sonicated silk fibroin.

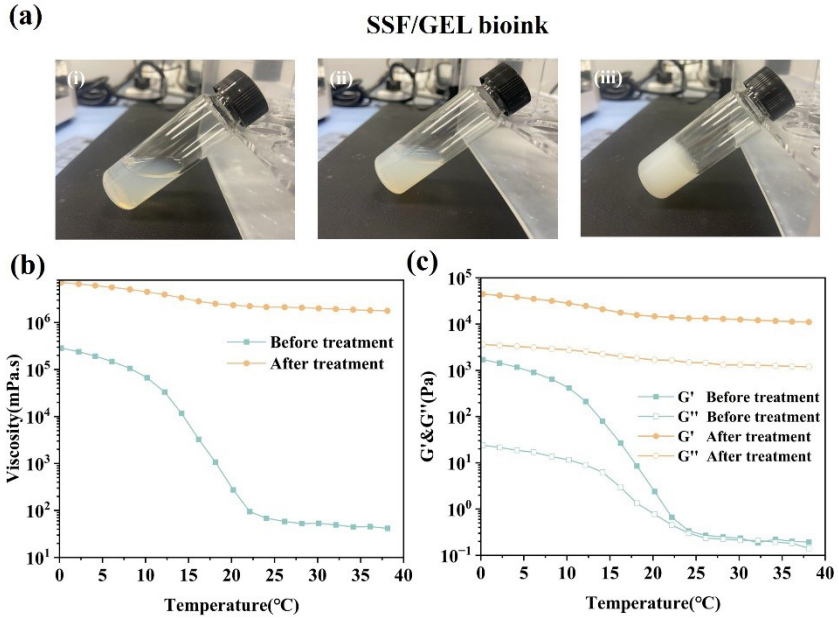

Figure 3. Effect of ultrasound treatment on the rheological properties of the ink. (a) Sol-gel transition of the ink at different times after ultrasound treatment: 0 h (i), 3 h (ii), and 5 h (iii); (b) Temperature sweep modulus analysis of 2SSF/1.5GEL ink before and after ultrasound treatment; (c) Temperature sweep viscosity analysis of 2SSF/1.5GEL ink before and after ultrasound treatment.
Abbreviations: G′: Storage modulus; G″: Loss modulus; GEL: Gelatin; SSF: Sonicated silk fibroin.

(hydroxyapatite: 5 wt%–20 wt%) were developed (Figure 4a). The printability of inks with different ratios was evaluated through rheological tests (Figure 4b–d). The results show that in the amplitude sweep test, the storage modulus (G′) of all inks was higher than the loss modulus (G″), indicating that the system exhibited significant solid-like characteristics. With the increase in oscillatory strain, the two gradually approached, suggesting that the network structure was destroyed and flow behavior began. In the rotational sweep test, all inks exhibited shear-thinning properties—maintaining high viscosity at low shear rates and undergoing a significant viscosity reduction with increasing shear rates. This rheological profile is conducive to simulating the extrusion behavior of bioinks during 3D printing, as it enables smooth filament extrusion under shear force while preserving structural integrity post-extrusion. Collectively, these findings confirmed that all developed bioinks possessed prominent solid-like characteristics and shear-thinning properties, which were indispensable prerequisites for satisfactory printability of bioinks in 3D bioprinting.

With the increase in gelatin concentration, the structural fidelity of the printed scaffolds showed an increasing trend (Figure 4b). The 3SSF/1GEL scaffold displayed the lowest printing fidelity, with the scaffold exhibiting phenomena of filament breakage and uneven filament extrusion. Rheological analysis revealed that the 3SSF/1GEL bioink exhibited inferior modulus and viscosity, which compromised the shape retention capability of the printed scaffold and thus led to unsatisfactory printing performance. As the gelatin concentration increased, the storage modulus (G′), loss modulus (G″), and viscosity of the bioinks were significantly enhanced, resulting in improved structural fidelity of the corresponding scaffolds. This can be attributed to the elevated protein concentration in the bioink: the increase in protein content facilitated the enhancement of intermolecular crosslinking density, rendering the internal network structure of the bioink more stable and thereby optimizing the printability and molding quality of the scaffolds. Among all formulations, the 3SSF/1.5GEL scaffold presented the most well-defined structural morphology.

With the gelatin concentration fixed at 1.5% w/v, the printed scaffolds fabricated with different SF concentrations (2SSF/1.5GEL, 2.5SSF/1.5GEL, and 3SSF/1.5GEL) demonstrated excellent structural integrity without filament breakage, indicating that these bioinks possessed favorable printability. Rheological characterization showed that the storage modulus (G′), loss modulus (G″), and viscosity of the bioinks increased progressively with increasing SF concentration (Figure 4c). This phenomenon was attributed to the enhanced intermolecular crosslinking density induced by the increased SF content, which in turn improved the mechanical strength and viscosity of the

bioink matrices.

A small amount of nano-hydroxyapatite (nHAP) particles can be uniformly dispersed in the SF-gelatin system, and both 3SSF/1.5GEL/5HAP and 3SSF/1.5GEL/10HAP exhibited good printability. With the increase in HAP concentration, the storage modulus (G′), loss modulus (G″), and viscosity of the inks increased significantly (Figure 4d). This may be due to the enhanced intermolecular and interfacial interactions between nHAP particles and the SSF/GEL polymer chains with increasing nHAP content, which consequently improved the viscosity and modulus of the composite system.[40] However, when the nHAP concentration was elevated to 20 wt%, filament breakage and uneven extrusion were observed during printing. Excessively high nHAP concentration may lead to particle agglomeration and heterogeneous dispersion within the bioink matrix, thereby causing nozzle clogging and impairing the printability of the bioink.[41]

To clarify the effect of high-pressure sterilization on the printability of the bioink, the rheological properties and scaffold forming performance of the bioink before and after high-pressure sterilization were compared in this study, with rheological tests conducted on the bioink subsequent to its gelation. The results show no significant differences in the modulus and viscosity of the bioink, and the solid-state characteristics and shear-thinning behavior remained consistent (Figure S1a and S1c, in Supplementary File). Meanwhile, no remarkable differences were observed in the structural fidelity of the 3D-printed scaffolds for both the cartilage and bone layers before and after sterilization (Figure S1b and S1d, in Supplementary File). Collectively, these findings confirm that this ultrasonic sterilization

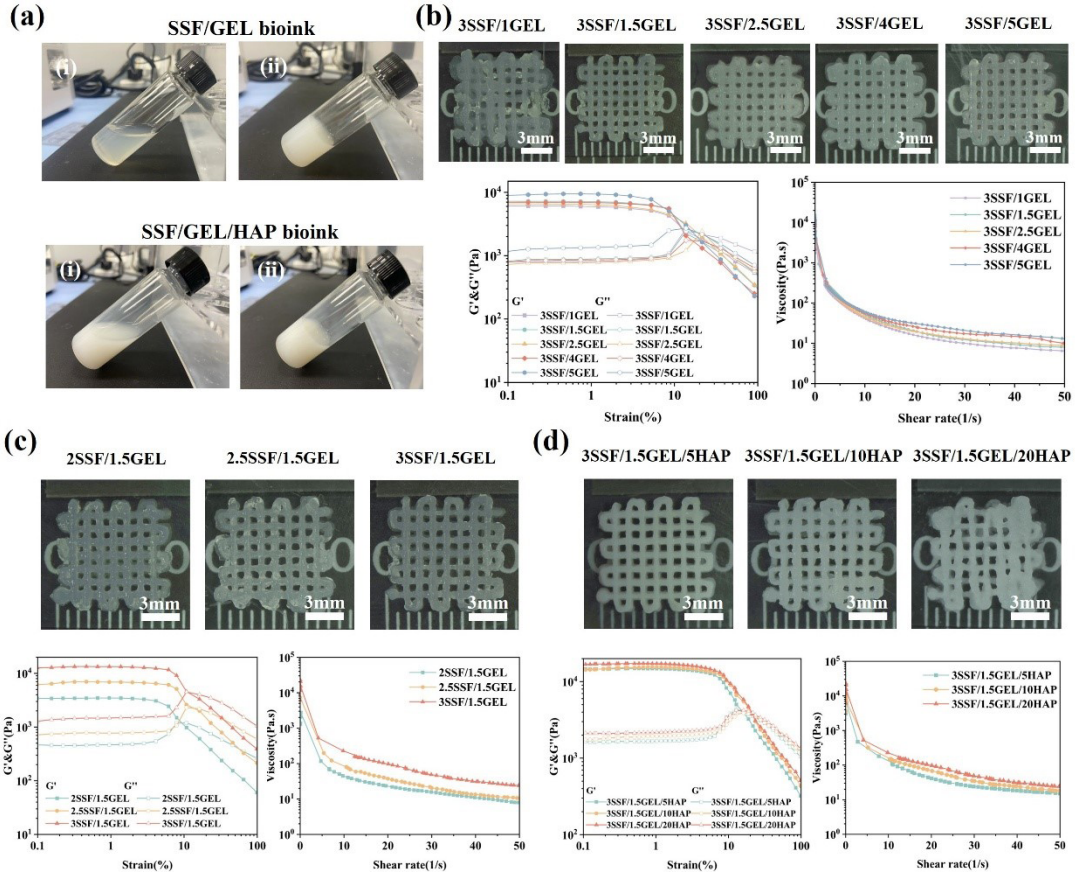

Figure 4. Rheological properties and printability of bioinks under different component concentrations. (a) The states of the cartilage layer (upper) and the bone layer (lower) ink before (i) and after gelation (ii); (b) Printed scaffolds of bioinks with different gelatin concentrations, along with their oscillatory amplitude sweeps (left) and rotational shear rate sweeps (right). (c) Printed scaffolds with different silk fibroin concentrations, as well as oscillatory amplitude sweeps (left) and rotational shear rate sweeps (right); (d) Printed scaffolds with different hydroxyapatite concentrations, together with oscillatory amplitude sweeps (left) and rotational shear rate sweeps (right).
Abbreviations: GEL: Gelatin; HAP: Hydroxyapatite; SSF: Sonicated silk fibroin.

process exerts no adverse effects on the printability of the bioink, thereby providing a reliable guarantee for subsequent 3D bioprinting of scaffolds and relevant biological experiments.

3.3. Characterization of bilayer scaffolds

In this study, a bilayer scaffold constructed from SSF/GEL and SSF/GEL/HAP bioinks was designed (Figure 5a). The SSF/GEL bioink was loaded with ATDC5 cells for printing the cartilage layer to facilitate chondrogenic matrix formation, while the SSF/GEL/HAP bioink was used to mimic the bone layer, with HAP incorporation to induce osteogenic differentiation of BMSCs. Gelatin without chemical crosslinking undergoes significant swelling and drastic volume changes, making it difficult to maintain the scaffold structure stability. To construct an integrated osteochondral scaffold with a stable structure and avoid delamination at the osteochondral interface, inks with similar swelling ratios should be selected.[42] A series of scaffolds were fabricated, and their structures and filament diameters were characterized (Figure 5).

The printed scaffolds were immersed in PBS at 37 °C to evaluate their structural stability (Figure 5b). The results showed that only the 3SSF/5GEL scaffold exhibited structural damage after immersion (Figure S2, in Supplementary File), and all other groups maintained good stability. This phenomenon may be attributed to the excessively high gelatin content in the 3SSF/5GEL bioink. As the temperature increased, the number of hydrogen bonds decreased sharply, leading to the transition of gelatin from a gel state to a sol state.[43] The presence of the SF network constrained the mobility of gelatin molecules, when the gelatin content was low enough, the scaffold structure was preserved, enabling the remaining scaffolds to maintain structural stability in PBS at 37 °C.

Quantitative statistical analysis of the filament diameters of the cartilage layer and bone layer scaffolds before and after immersion in PBS at 37 °C was performed. No significant changes in filament diameter were observed for all scaffolds before and after PBS immersion (Figure 5c). This may be attributed to the constraint imposed by the SF crosslinked network structure. After ultrasonic treatment, SF with a high β-sheet content forms a rigid network, which restricts the lateral expansion of the material.[44] The modulus of both the cartilage layer and bone layer bioinks remained overall stable with a slight decrease as the temperature increased (Figure 5d), indicating that the scaffold performance was less affected by gelatin and exhibited low temperature sensitivity. The low swelling property and thermosensitivity of these scaffolds facilitated

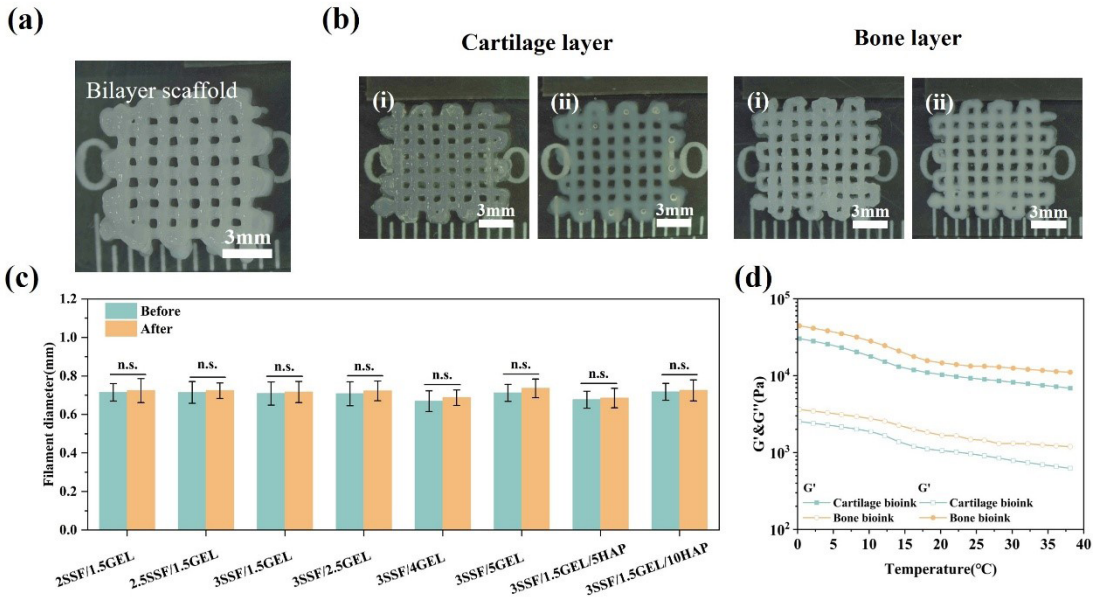

Figure 5. Structural stability and self-healing properties of silk fibroin/gelatin scaffolds. (a) Top view of the bilayer scaffold; (b) Morphology of the cartilage layer scaffold (2SSF/1.5GEL) and bone layer scaffold (3SSF/1.5GEL/10HAP) before (i) and after immersion in 37 °C PBS solution (ii); (c) Fiber diameters of different 3D-printed scaffolds before and after PBS immersion; (d) Oscillatory amplitude temperature sweep tests of the cartilage layer bioink (2SSF/1.5GEL) and bone layer bioink (3SSF/1.5GEL/10HAP).
Abbreviations: GEL: Gelatin; HAP: Hydroxyapatite; PBS: Phosphate-buffered saline; SSF: Sonicated silk fibroin.

the construction of a bilayer scaffold with stable interfaces, preventing interfacial sliding of the printed biphasic scaffold caused by the mismatch in swelling ratios between the upper- and lower-layer components.

Long-term structural stability of the scaffolds is a critical prerequisite for subsequent biological experiments. In this study, the prepared scaffolds were subjected to a simulated physiological environment via immersion in 37 °C PBS solution for one week, which confirmed that the scaffolds could maintain an intact and stable structure (Figure S3, in Supplementary File), thus meeting the structural requirements for scaffolds in biological experiments.

When fabricating the upper and lower heterogeneous bilayer scaffolds, the self-healing ability of the bioinks (based on a reversible crosslinking mechanism) enables the spontaneous filling of interfacial micro-gaps, buffering of interlayer stress to avoid stress accumulation, and improvement of interfacial contact defects caused by process fluctuations. This ability effectively inhibits interfacial delamination between the upper and lower scaffold layers, and serves as a critical property for ensuring the structural stability of the heterogeneous scaffolds.

Rheological self-healing tests verified the self-repairing capacity of the core bioinks. The cartilage layer (2SSF/1.5GEL) and bone layer (3SSF/1.5GEL/10HAP) bioinks exhibited a typical gel state at low strain (1%). When subjected to large deformation (100%), the internal crosslinking network was disrupted and the storage modulus (G′) rapidly decreased to a value lower than the loss modulus (G″). Upon the recovery of strain to 1%, both G′ and G″ quickly reverted to their initial values (Figure 6a and 6b), which demonstrates the efficient self-healing properties of the cartilage layer (2SSF/1.5GEL) and bone layer (3SSF/1.5GEL/10HAP) bioinks.

After the two cut hydrogel sections were brought into contact, they were left to stand at room temperature for a period of time. The gap at the bonding interface gradually vanished, and an intact, continuous hydrogel was eventually reconstituted. The healed hydrogel could withstand mild external tensile stretching (it could be lifted by fixing one end) without fracture at the bonded site, which confirmed that its macroscopic structure had undergone effective repair and possessed a certain degree of self-healing integrity (Figure 6c–e). Gelatin molecules contain abundant amino and hydroxyl groups, which can form hydrogen bonds with hydroxyl groups, amide groups, and other functional groups in gelatin and SF molecules. When the hydrogel structure is damaged, these broken hydrogen bonds can re-form through the thermal motion of molecular chains and the reapproximation of polar groups, further complementing the repair of the crosslinked network and enhancing the stability and integrity of the self-healing effect.[39,45] Furthermore, studies have demonstrated that SF can form a crosslinked network via the β-sheet conformation, endowing the material with excellent self-healing capacity.[46,47] This self-healing property facilitates the tight interfacial bonding of SF-based bilayer scaffolds, precluding structural delamination.

3.4. Mechanical properties and structural characteristics of bilayer scaffolds

The mechanical microenvironment of a scaffold governs pivotal biological processes—including proliferation and lineage-specific differentiation of resident cells—and is therefore a critical determinant of successful osteochondral regeneration. To systematically refine the ink formulation of bilayer scaffold, compressive property tests were performed on the cartilage layer and bone layer scaffolds separately. With the increase in SF content, the compressive modulus increased correspondingly, from 4.15 ± 0.89 kPa to 11.41 ± 0.53 kPa (Figure 7a and 7b). Silk fibroin, the dominant structural protein, self-assembles into a denser network as its concentration rises, driven by intensified intermolecular hydrogen bonding and β-sheet crosslinking. This nano-structural reinforcement translates directly into enhanced resistance to mechanical loading.[48,49] For the bone layer scaffolds, the compressive modulus increased significantly with the increase in HAP content, reaching a maximum value of 16.69 ± 1.54 kPa at a content of 10%. However, when the HAP content increased to 20%, the compressive modulus decreased to 11.15 ± 2.27 kPa (Figure 7c and 7d). This phenomenon may be associated with the printability of the bioink, filament breakage of the scaffolds compromised structural uniformity, thereby impairing mechanical performance.

Early in chondrogenesis, low-stiffness matrices (~3–5 kPa) promote actin cytoskeletal disassembly and a rounded cell morphology, thereby facilitating chondrogenic commitment of mesenchymal stromal cells (MSCs).[50] Conversely, high moduli (~17 kPa) activate osteogenic signaling cascades and markedly enhance osteogenic differentiation efficiency.[51] Guided by these mechanobiological thresholds—and ensuring comparable swelling ratios—we selected 2SSF/1.5GEL (4.15 ± 0.89 kPa) for the cartilaginous layer and 3SSF/1.5GEL/10HA (16.69 ± 1.54 kPa) for the osseous layer for all subsequent biological evaluations.

To evaluate the structural stability of the scaffolds under dynamic loading, their elastic recovery properties were investigated via loading–unloading cyclic compression tests. The results showed that both the 2SSF/1.5GEL scaffold and the 3SSF/1.5GEL/10HAP scaffold could

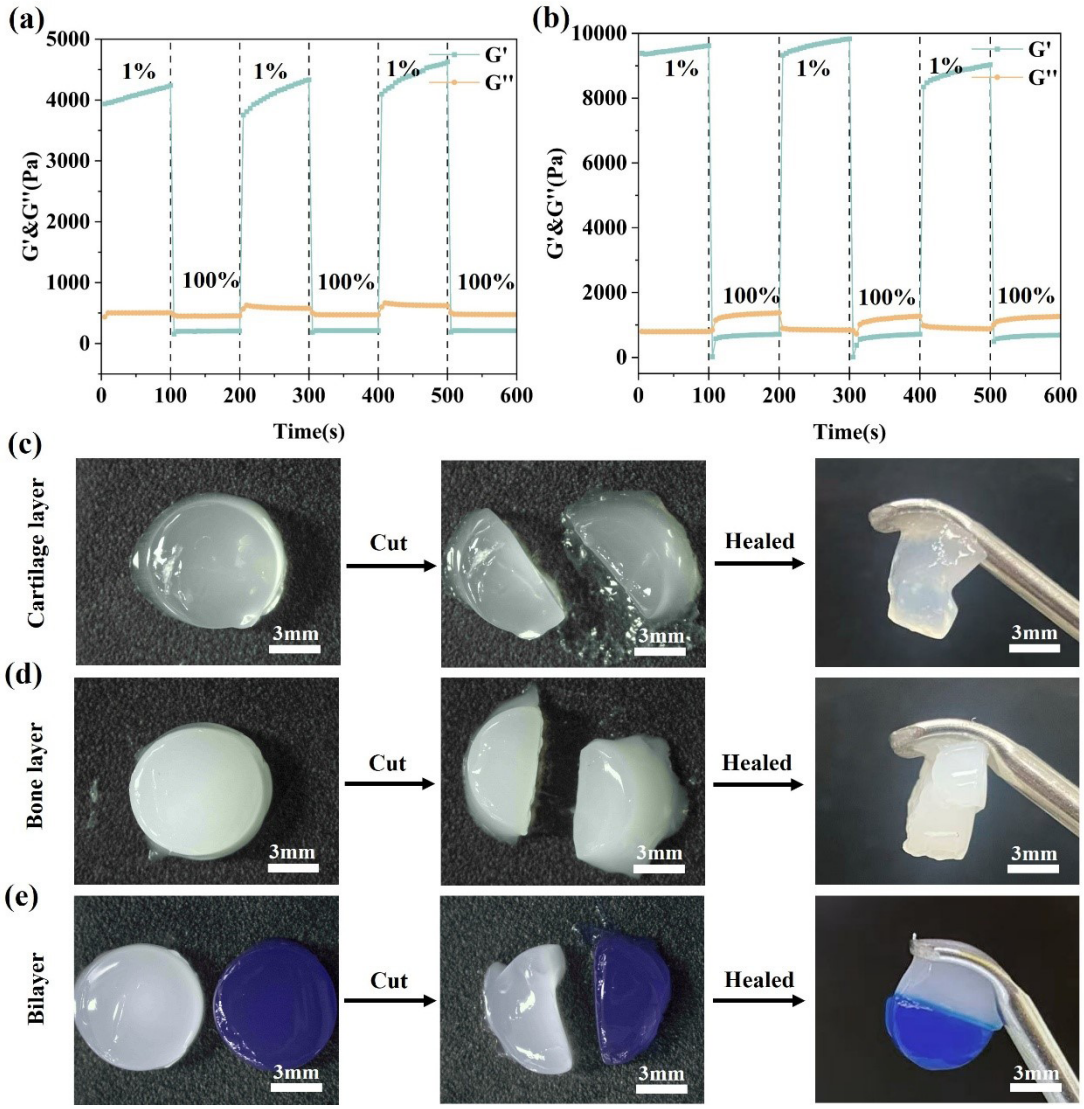

Figure 6. Self-healing behaviors of the osteochondral layer bioinks. (a) Rheological self-healing test of the cartilage layer bioink (2SSF/1.5GEL); (b) Rheological self-healing test of the bone layer bioink (3SSF/1.5GEL/10HAP) with alternating strains from 1% to 100%; (c) Self-healing process of the cartilage layer bioink material (2SSF/1.5GEL); (d) Self-healing process of the bone layer bioink material (3SSF/1.5GEL/10HAP); (e) Self-healing process after splicing of the cartilage layer material (2SSF/1.5GEL, white) and the bone layer material (3SSF/1.5GEL/10HAP, blue).
Abbreviations: G′: Storage modulus; G″: Loss modulus; GEL: Gelatin; HAP: Hydroxyapatite; SSF: Sonicated silk fibroin.

stably withstand 25% compressive strain. The curves after the second loading cycle exhibited good repeatability, confirming that the scaffolds maintained stable elastic recovery under repeated loading. The residual strain of the 2SSF/1.5GEL scaffold was approximately 20% (Figure 7e), corresponding to a height recovery of about 80% after compression (Figure S4, in Supplementary File). For the 3SSF/1.5GEL/10HAP scaffold, the residual strain was approximately 15% (Figure 7f), with a height recovery of about 85% (Figure S4, in Supplementary File). This limited immediate recovery can be attributed to the release of interstitial water and structural densification of the hydrogel under high compressive stress, which hindered full elastic recovery. In addition, the compressive stress retention rates of the two scaffolds relative to the initial stress were 85.6% and 84.7%, respectively (Table S1, in Supplementary File), further demonstrating their excellent structural stability. Notably, after immersion in PBS, the height recovery rates of both the cartilage layer and bone layer scaffolds increased to 95%, indicating that their elastic recovery was significantly restored in an aqueous environment (Figure S4, in Supplementary File).

Microscopic inspection of the bilayer interface revealed a macroscopically intact construct (Figure 7g, left). Scanning electron microscopy (SEM) micrographs of the scaffold cross-section exhibited robust interfacial integration between the two layers without any signs of delamination (Figure 7g). High-magnification SEM images of the scaffold surface revealed that the upper layer displayed a smooth topographical feature, whereas the lower layer surface was uniformly decorated with HAP particles (Figure S5, in Supplementary File), demonstrating the successful fabrication of an integrated scaffold with heterogeneous compositions. This heterogeneous design enables biomimetic replication of the mechanical properties of native osteochondral tissue, thereby providing an integrated structural and functional platform for osteochondral regeneration.

3.5. *In vitro* biological analysis of bilayer scaffolds

In this study, qualitative and quantitative analyses of cell viability were performed. For the cartilage layer scaffold, ATDC5 cells were homogenously mixed with the SSF/GEL bioink prior to 3D bioprinting (Figure 8a); for the bone layer scaffold, the BMSCs were seeded onto the pre-printed SSF/GEL/HAP scaffold (Figure 8b). Live/dead staining assays revealed that both scaffolds (cartilage layer and bone layer) exhibited a high viable cell ratio and minimal dead cells, achieving a cell viability rate of over 90% (Figure S6, in Supplementary File). In the cartilage layer scaffold, cells were uniformly dispersed throughout the scaffold on day 1. After 7 days of culture, the green fluorescence intensified and filled the entire scaffold (Figure 8c(i)), indicating that the cartilage layer scaffold created a favorable

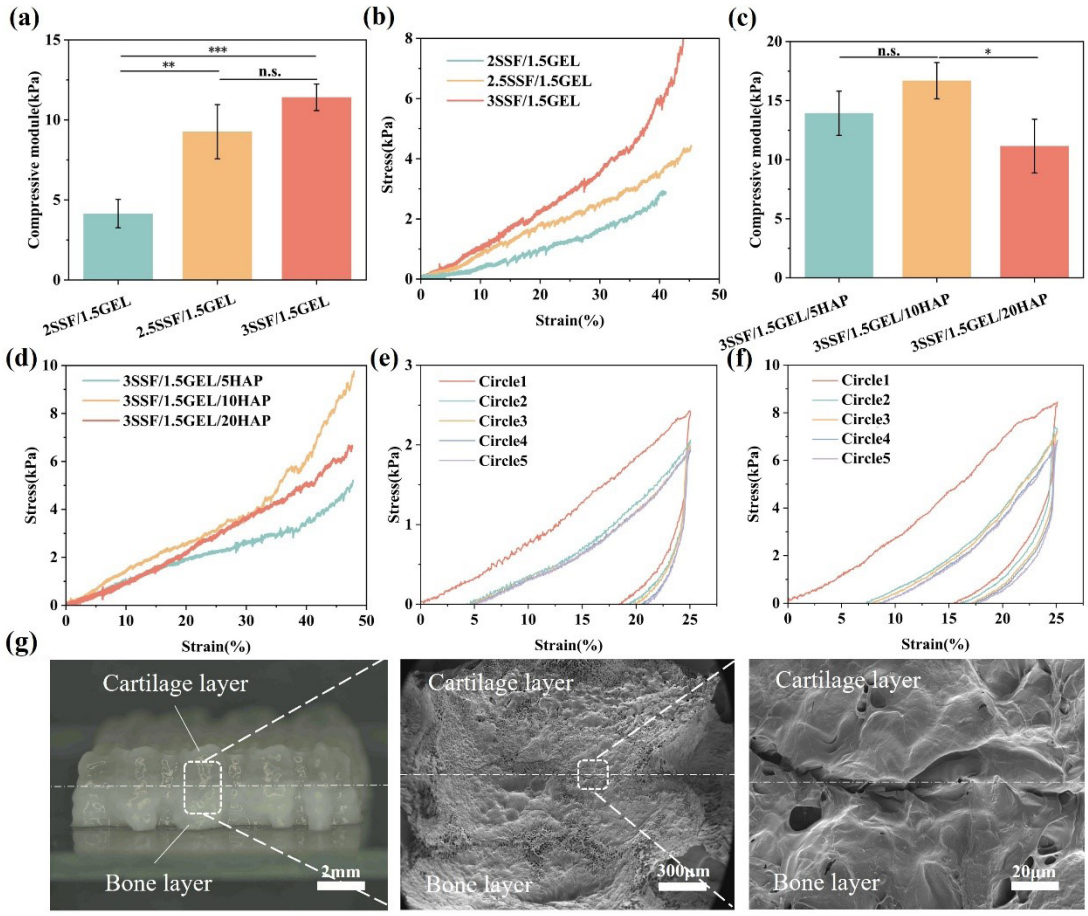

Figure 7. Mechanical properties and structural characteristics of the scaffolds. (a) Compressive modulus of cartilage-layer scaffolds with different silk fibroin concentrations; (b) Stress–strain curves; (c) Compressive modulus of bone-layer scaffolds with different hydroxyapatite concentrations ($n = 3$; $^{*}p \leq 0.05$, $^{**}p \leq 0.01$, $^{***}p \leq 0.001$); (d) Stress–strain curves; (e) Cyclic loading test of cartilage-layer scaffold (2SSF/1.5GEL); (f) Cyclic loading test of bone-layer scaffold (3SSF/1.5GEL/10HAP); (g) Macrostructure of the bilayer scaffold and scanning electron microscopy image of the interface.
Abbreviations: GEL: Gelatin; HAP: Hydroxyapatite; SSF: Sonicated silk fibroin.

microenvironment for ATDC5 cells. In the bone layer scaffold, green fluorescent spots were mainly concentrated on the scaffold surface on day 1, with no obvious fluorescent signal detected inside the scaffold. After 7 days of culture, the cells gradually migrated into the scaffold interior, and the fluorescence intensity increased significantly, covering most areas (Figure 8c(ii)). This indicated that the number of BMSCs in the bone layer scaffold increased, and the cells exhibited a tendency to migrate inward and grow. Furthermore, quantitative analysis of cell bioactivity on the cartilage layer and bone layer scaffolds via the CCK-8 assay (Figure 8d) showed that the OD values of both scaffolds increased gradually with the extension of culture time. These results indicate that both the bone layer and cartilage layer scaffolds possess good biocompatibility. The use of physically crosslinked SSF/GEL cartilage ink for cell-laden 3D printing is feasible, which can maintain high viability and proliferation capacity of chondrocytes.

To evaluate the bidirectional differentiation potential of the bilayer scaffolds, immunofluorescence staining and fluorescence intensity analysis for type II collagen and RUNX2 were performed on the cartilage layer scaffolds, bone layer scaffolds and bilayer scaffolds after 7 days of culture (Figure 9a). The results show strong expression of type II collagen in the cartilage layer scaffold, which was distributed throughout the printed fibers, while no RUNX2 signal was detected, indicating a typical chondrocyte phenotype. Type II collagen is the most abundant collagen in the mature cartilage matrix. It forms a fibrous network through self-assembly, providing basic physical structural support for cartilage tissue and maintaining the morphology and integrity of cartilage. The expression of type II collagen confirms that the cells have activated the chondrogenic differentiation process, progressively gaining the phenotypic traits of chondrocytes. In contrast, the bone layer scaffold exhibited significant RUNX2 expression, with particularly high fluorescence intensity on the filament surfaces, while only weak type II collagen expression was detected, which is consistent with the phenotypic characteristics of osteoblasts. In the bilayer composite

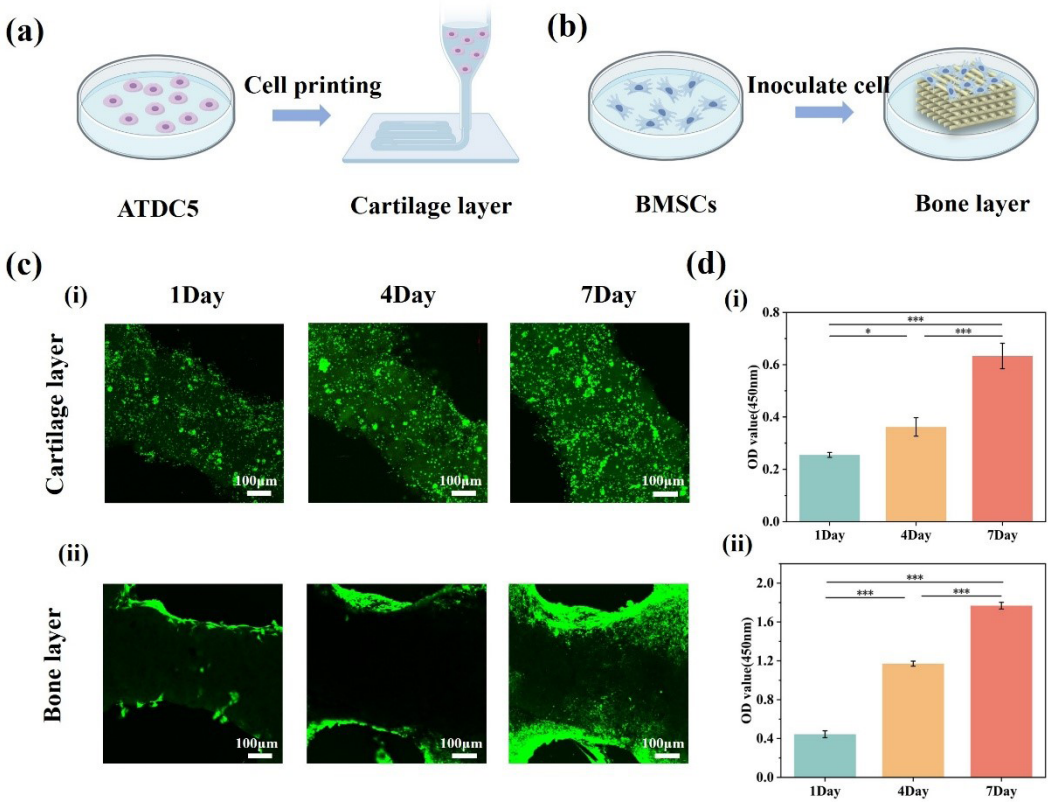

Figure 8. Evaluation of the biocompatibility of the osteochondral bilayer scaffold. (a) Schematic illustration of cartilage layer scaffolds printed with ATDC5 cell-laden bioink; (b) Schematic illustration of bone layer scaffolds seeded with BMSCs; (c) Live/dead staining of cartilage layer scaffolds (2SSF/1.5GEL, panel i) and bone layer scaffolds (3SSF/1.5GEL/10HAP, panel ii); (d) Cell viability (OD values) of cartilage layer scaffolds (2SSF/1.5GEL, panel i) and bone layer scaffolds (3SSF/1.5GEL/10HAP, panel ii) on days 1, 4 and 7 ($n = 3$; $p \leq 0.05$, $p \leq 0.01$, $p \leq 0.001$).
Abbreviations: BMSCs: Bone marrow-derived mesenchymal stem cells; GEL: Gelatin; HAP: Hydroxyapatite; SSF: Sonicated silk fibroin.

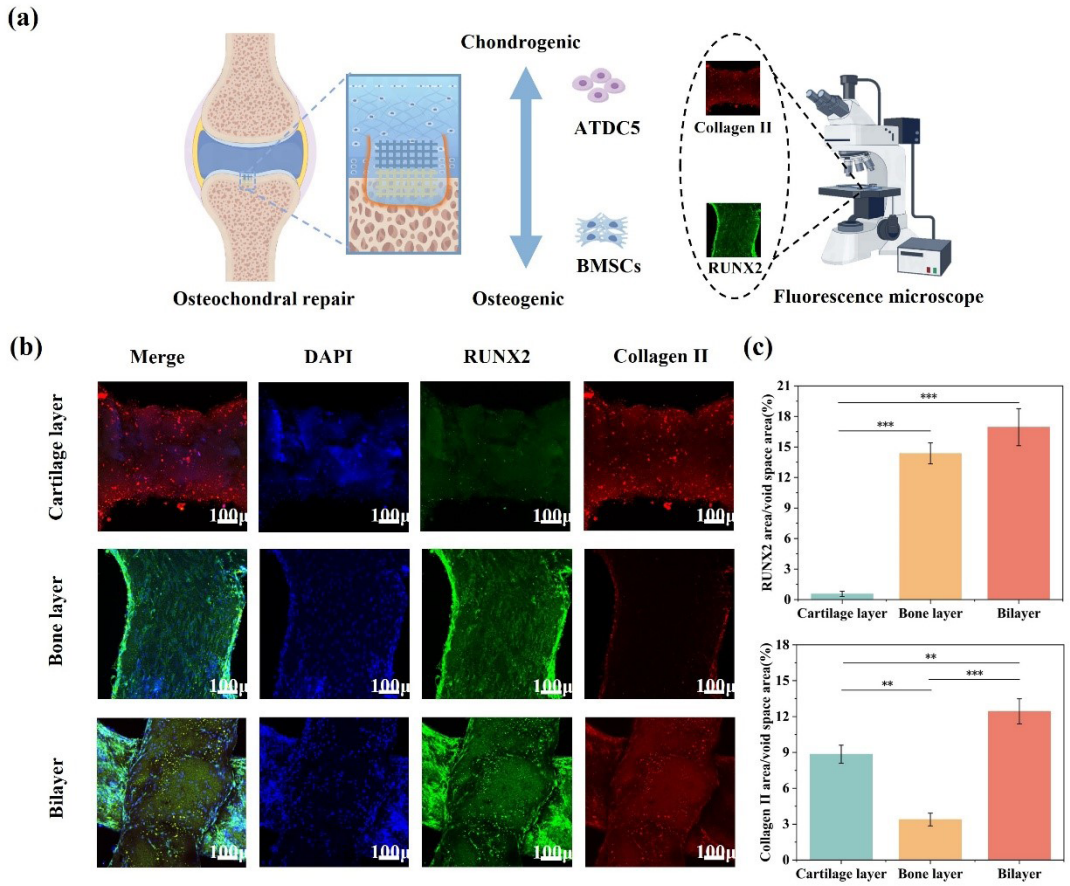

Figure 9. Immunofluorescence staining of the double-layer scaffold. (a) Repair mechanism for osteochondral defect and expression of related markers; (b, c) Double immunofluorescence staining and fluorescence intensity analysis of chondrogenic differentiation marker type II collagen and osteogenic differentiation marker RUNX2 in cartilage layer (2SSF/1.5GEL), bone layer (3SSF/1.5GEL/10HAP) and combined bilayer scaffolds at day 7 of culture.
Abbreviations: BMSCs: Bone marrow-derived mesenchymal stem cells; GEL: Gelatin; HAP: Hydroxyapatite; SSF: Sonicated silk fibroin.

scaffold, the cartilage layer and bone layer maintained high type II collagen and RUNX2 expression in their respective regions, respectively (Figure 9b and 9c). Therefore, we conclude that the SSF/GEL and SSF/GEL/HAP bioinks are highly feasible for constructing osteochondral scaffolds. ATDC5 cells and BMSCs can be co-cultured, exhibiting excellent bidirectional differentiation effects, and achieving chondrogenic differentiation and osteogenic differentiation in the bilayer scaffold respectively.

4. Conclusion

A physically crosslinked silk fibroin-gelatin bioink tailored for cell-laden 3D bioprinting was developed via precise regulation of gelation kinetics through ultrasonic treatment. Synergistic effect between the self-assembly behavior of silk fibroin and the high viscosity of gelatin endowed the SSF/GEL ink with excellent printability and structural stability. Incorporating nano-hydroxyapatite yielded an osteoinductive SSF/GEL/HAP bone layer bioink. These physically crosslinked bioinks, featuring tunable mechanics, intrinsic self-healing, and biocompatibility, enabled fabrication of bilayer osteochondral scaffolds with intimate interfacial integration. Functionally, the cartilage layer supported chondrogenic differentiation of encapsulated ATDC5 cells, while the bone layer promoted region-specific osteogenic commitment of BMSCs. This work presents a clinically translatable material platform and facile 3D bioprinting strategy, offering a promising alternative for complex osteochondral defect repair.

Acknowledgments

None.

Funding

This work was supported by the National Key Research and Development Program of China (2022YFA1104600); the

Zhejiang Provincial Natural Science Foundation of China (LY24A020006); the Key Research and Development Foundation of Zhejiang Province (2024C03068); the Key Research and Development Foundation of Hangzhou City (2024SZD1B07); the National Natural Science Foundation of China (12002112); and the Central Government Guiding Funds for Local Science and Technology Development (2025ZY01048).

Conflict of interest

Mingen Xu serves as an Editorial Board Member of the journal, but did not in any way involve in the editorial and peer-review process conducted for this paper, directly or indirectly. Other authors declare they have no competing interests

Author contributions

Conceptualization: Danyu Yao, Ling Wang, Mingen Xu
Investigation: Hong Liu
Methodology: Danyu Yao, Hong Liu
Formal analysis: Danyu Yao, Hong Liu
Writing–original draft: Hong Liu, Danyu Yao
Writing–review & editing: Danyu Yao, Ling Wang, Mingen Xu

Ethics approval and consent to participate

Not applicable.

Consent for publication

Not applicable.

Availability of data

Data are available from the corresponding author upon reasonable request.

References

1. Long H, Liu Q, Yin H, *et al*. Prevalence trends of site-specific osteoarthritis from 1990 to 2019: findings from the Global Burden of Disease Study 2019. *Arthritis Rheumatol*. 2019;74(7):1172-1183.

   doi: 10.1002/art.42089

2. Yang M, Zhang ZC, Yuan FZ, *et al*. An immunomodulatory polypeptide hydrogel for osteochondral defect repair. *Bioact Mater*. 2023;19:678-689.

   doi: 10.1016/j.bioactmat.2022.05.008

3. Wu Z, Yao H, Sun H, *et al*. Enhanced hyaline cartilage formation and continuous osteochondral regeneration via 3D-Printed heterogeneous hydrogel with multi-crosslinking inks. *Mater Today Bio*. 2024;26:101080.

   doi: 10.1016/j.mtbio.2024.101080

4. Li M, Yin H, Yan Z, *et al*. The immune microenvironment in cartilage injury and repair. *Acta Biomater*. 2022;140:23-42.

   doi: 10.1016/j.actbio.2021.12.006

5. Singh YP, Bandyopadhyay A, Mandal BB. 3D bioprinting using cross-linker-free silk–gelatin bioink for cartilage tissue engineering. *ACS Appl Mater Interfaces*. 2019;11(37):33684-33696.

   doi: 10.1021/acsami.9b11644

6. Li C, Zhang W, Nie Y, *et al*. Integrated and bifunctional bilayer 3D printing scaffold for osteochondral defect repair. *Adv Funct Mater*. 2023;33(20):2214158.

   doi: 10.1002/adfm.202214158

7. Lowen JM, Wheeler EE, Shimamoto NK, *et al*. Functionalized annealed microgels for spatial control of osteogenic and chondrogenic differentiation. *Adv Funct Mater*. 2024;34(30):2311017.

   doi: 10.1002/adfm.202311017

8. Lee J, Lee S, Huh SJ, Kang BJ, Shin H. Directed regeneration of osteochondral tissue by hierarchical assembly of spatially organized composite spheroids. *Adv Sci*. 2022;9(3):2103525.

   doi: 10.1002/advs.202103525

9. Wang H, Zhang J, Bai H, *et al*. 3D printed cell-free bilayer porous scaffold based on alginate with biomimetic microenvironment for osteochondral defect repair. *Biomater Adv*. 2025;167:214092.

   doi: 10.1016/j.bioadv.2024.214092

10. Levingstone TJ, Matsiko A, Dickson GR, O'Brien FJ, Gleeson JP. A biomimetic multi-layered collagen-based scaffold for osteochondral repair. *Acta Biomater*. 2014;10(5):1996-2004.

    doi: 10.1016/j.actbio.2014.01.005

11. Shimomura K, Moriguchi Y, Murawski CD, Yoshikawa H, Nakamura N. Osteochondral tissue engineering with biphasic scaffold: current strategies and techniques. *Tissue Eng Part B Rev*. 2014;20(5):468-476.

    doi: 10.1089/ten.teb.2013.0543

12. Barui S, Ghosh D, Laurencin CT. Osteochondral regenerative engineering: challenges, state-of-the-art and translational perspectives. *Regen Biomater*. 2023;10:rbac109.

    doi: 10.1093/rb/rbac109

13. Du J, Zhu Z, Liu J, *et al*. 3D-printed gradient scaffolds for osteochondral defects: Current status and perspectives. *Int J Bioprint*. 2023;9(4):724.

    doi: 10.18063/ijb.724

14. Lai Y, Fan J, Li P, *et al*. Recent advances in 3D bioprinting for cartilage and osteochondral regeneration. *Int J Bioprint*. 2025;11(3):154-184.

    doi: 10.36922/IJB025120098

15. Huey DJ, Hu JC, Athanasiou KA. Unlike bone, cartilage regeneration remains elusive. *Science*. 2012;338(6109):917-921.

doi: 10.1126/science.1222454

16. Niu X, Li N, Du Z, Li X. Integrated gradient tissue-engineered osteochondral scaffolds: Challenges, current efforts and future perspectives. *Bioact Mater*. 2023;20:574-597.

doi: 10.1016/j.bioactmat.2022.06.011

17. Li C, Guo C, Fitzpatrick V, *et al*. Design of biodegradable, implantable devices towards clinical translation. *Nat Rev Mater*. 2020;5(1):61-81.

doi: 10.1038/s41578-019-0150-z

18. Sarr MM, Inoue H, Kosaka T. Study on the improvement of interfacial strength between glass fiber and matrix resin by grafting cellulose nanofibers. *Compos Sci Technol*. 2021;211:108853.

doi: 10.1016/j.compscitech.2021.108853

19. Sharifi S, Islam MM, Sharifi H, *et al*. Tuning gelatin-based hydrogel towards bioadhesive ocular tissue engineering applications. *Bioact Mater*. 2021;6(11):3947-3961.

doi: 10.1016/j.bioactmat.2021.03.042

20. Zhang X, Liu Y, Zuo Q, *et al*. 3D bioprinting of biomimetic bilayered scaffold consisting of decellularized extracellular matrix and silk fibroin for osteochondral repair. *Int J Bioprint*. 2021;7(4):401.

doi: 10.18063/ijb.v7i4.401

21. Chawla S, Midha S, Sharma A, Ghosh S. Silk-based bioinks for 3D bioprinting. *Adv Healthc Mater*. 2018;7(8):1701204.

doi: 10.1002/adhm.201701204

22. Kim SH, Yeon YK, Lee JM, *et al*. Precisely printable and biocompatible silk fibroin bioink for digital light processing 3D printing. *Nat Commun*. 2018;9(1):1620.

doi: 10.1038/s41467-018-03759-y

23. Kokol V, Pottathara YB, Mihelčič M, Perše LS. Rheological properties of gelatine hydrogels affected by flow- and horizontally-induced cooling rates during 3D cryo-printing. *Colloids Surf A Physicochem Eng Asp*. 2021;616:126356.

doi: 10.1016/j.colsurfa.2021.126356

24. Hou P, Yang X, Liu Z, *et al*. Advancing knee cartilage repair with 3D printed GelMA/SF/Haps composite hydrogels for enhanced chondrocyte regeneration. *J Mater Sci*. 2024;59(11):4636-4648.

doi: 10.1007/s10853-024-09508-5

25. Zheng Z, Wu J, Liu M, *et al*. 3D bioprinting of self-standing silk-based bioink. *Adv Healthc Mater*. 2018;7(6):1701026.

doi: 10.1002/adhm.201701026

26. Zou S, Fan S, Oliveira AL, *et al*. 3D printed gelatin scaffold with improved shape fidelity and cytocompatibility by using Antheraea pernyi silk fibroin nanofibers. *Adv Fiber Mater*. 2022;4(4):758-773.

doi: 10.1007/s42765-022-00135-w

27. Chakraborty J, Fernández-Pérez J, van Kampen KA, *et al*. Development of a biomimetic arch-like 3D bioprinted construct for cartilage regeneration using gelatin methacryloyl and silk fibroin-gelatin bioinks. *Biofabrication*. 2023;15(3):035009.

doi: 10.1088/1758-5090/acc68f

28. Lee H, Shin D, Shin S, Hyun J. Effect of gelatin on dimensional stability of silk fibroin hydrogel structures fabricated by digital light processing 3D printing. *J Ind Eng Chem*. 2020;89:119-127.

doi: 10.1016/j.jiec.2020.03.034

29. Chu S, Maples MM, Bryant SJ. Cell encapsulation spatially alters crosslink density of poly(ethylene glycol) hydrogels formed from free-radical polymerizations. *Acta Biomater*. 2020;109:37-50.

doi: 10.1016/j.actbio.2020.03.033

30. Yuan X, Li G, Huang L, *et al*. Hydroxypropyl chitin-oxidized chondroitin sulfate double-network hydrogel assists microfracture technique to enhance cartilage regeneration. *Mater Des*. 2024;238:112656.

doi: 10.1016/j.matdes.2024.112656

31. Yao D, Li M, Wang T, *et al*. Viscoelastic silk fibroin hydrogels with tunable strength. *ACS Biomater Sci Eng*. 2021;7(2):636-647.

doi: 10.1021/acsbiomaterials.0c01348

32. Ding X, Gao J, Yu X, *et al*. 3D-printed porous scaffolds of hydrogels modified with TGF-β1 binding peptides to promote in vivo cartilage regeneration and animal gait restoration. *ACS Appl Mater Interfaces*. 2022;14(14):15982-15995.

doi: 10.1021/acsami.2c00761

33. Song P, Li M, Zhang B, *et al*. DLP fabricating of precision GelMA/HAp porous composite scaffold for bone tissue engineering application. *Compos B Eng*. 2022;244:110163.

doi: 10.1016/j.compositesb.2022.110163

34. Wang X, Kluge JA, Leisk GG, Kaplan DL. Sonication-induced gelation of silk fibroin for cell encapsulation. *Biomaterials*. 2008;29(8):1054-1064.

doi: 10.1016/j.biomaterials.2007.11.003

35. Zhong J, Liu X, Wei D, *et al*. Effect of incubation temperature on the self-assembly of regenerated silk fibroin: A study using AFM. *Int J Biol Macromol*. 2015;76:195-202.

doi: 10.1016/j.ijbiomac.2015.02.045

36. Lu Q, Zhu H, Zhang C, *et al*. Silk self-assembly mechanisms and control from thermodynamics to kinetics. *Biomacromolecules*. 2012;13(3):826-832.

doi: 10.1021/bm201731e

37. Mosleh Y, de Zeeuw W, Nijemeisland M, *et al*. The structure–property correlations in dry gelatin adhesive films. *Adv Eng Mater*. 2021;23(1):2000716.

doi: 10.1002/adem.202000716

38. Sun X, Liang H, Wang H, *et al*. Silk fibroin/polyvinyl alcohol composite film loaded with antibacterial AgNP/polydopamine-modified montmorillonite; characterization and antibacterial properties. *Int J Biol Macromol*. 2023;251:126368.

doi: 10.1016/j.ijbiomac.2023.126368

39. Park S, Edwards S, Hou S, *et al*. A multi-interpenetrating network (IPN) hydrogel with gelatin and silk fibroin. *Biomater Sci*. 2019;7(4):1276-1280.

doi: 10.1039/c8bm01532e

40. Zhanbassynova A, Mukasheva F, Abilev M, *et al*. Impact of Hydroxyapatite on Gelatin/Oxidized Alginate 3D-Printed Cryogel Scaffolds. *Gels*. 2024;10(6):406.

doi: 10.3390/gels10060406

41. Kazemi M, Mirzadeh M, Esmaeili H, *et al*. Evaluation of the morphological effects of hydroxyapatite nanoparticles on the rheological properties and printability of hydroxyapatite/polycaprolactone nanocomposite inks and final scaffold features. *3D Print Addit Manuf*. 2024;11(1):132-142.

doi: 10.1089/3dp.2021.0292

42. Luo M, Chen M, Bai J, *et al*. A bionic composite hydrogel with dual regulatory functions for the osteochondral repair. *Colloids Surf B Biointerfaces*. 2022;219:112821.

doi: 10.1016/j.colsurfb.2022.112821

43. Choi DJ, Kho Y, Park SJ, *et al*. Effect of cross-linking on the dimensional stability and biocompatibility of a tailored 3D-bioprinted gelatin scaffold. *Int J Biol Macromol*. 2019;135:659-667.

doi: 10.1016/j.ijbiomac.2019.05.207

44. Ren YJ, Zhou ZY, Liu BF, Xu QY, Cui FZ. Preparation and characterization of fibroin/hyaluronic acid composite scaffold. *Int J Biol Macromol*. 2009;44(4):372-378.

doi: 10.1016/j.ijbiomac.2009.02.004

45. Hoque M, Alam M, Wang S, *et al*. Interaction chemistry of functional groups for natural biopolymer-based hydrogel design. *Mater Sci Eng R Rep*. 2023;156:100758.

doi: 10.1016/j.mser.2023.100758

46. Guo W, Gao X, Ding X, *et al*. Self-adhesive and self-healing hydrogel dressings based on quaternary ammonium chitosan and host-guest interacted silk fibroin. *Colloids Surf A Physicochem Eng Asp*. 2024;684:133145.

doi: 10.1016/j.colsurfa.2024.133145

47. Yu R, Yang Y, He J, Li M, Guo B. Novel supramolecular self-healing silk fibroin-based hydrogel via host–guest interaction as wound dressing to enhance wound healing. *Chem Eng J*. 2021;417:128278.

doi: 10.1016/j.cej.2020.128278

48. Koh RH, Kim J, Kim JU, *et al*. Bioceramic-mediated chondrocyte hypertrophy promotes calcified cartilage formation for rabbit osteochondral defect repair. *Bioact Mater*. 2024;40:306-317.

doi: 10.1016/j.bioactmat.2024.06.018

49. Pacheco MO, Aikman EL, Bagnis HK, *et al*. Degumming Time Governs Self-Assembled Silk Fibroin Hydrogel Properties through Molecular Weight and Amino Acid Composition. *Biomacromolecules*. 2025;26(8):5069-5085.

doi: 10.1021/acs.biomac.5c00506

50. Lee H, Gu L, Mooney DJ, Levenston ME, Chaudhuri O. Mechanical confinement regulates cartilage matrix formation by chondrocytes. *Nat Mater*. 2017;16(12):1243-1251.

doi: 10.1038/nmat4993

51. Song J, Chen C, Zhu S, *et al*. Processing bulk natural wood into a high-performance structural material. *Nature*. 2018;554(7691):224-228.

doi: 10.1038/nature25476